CHEMISTRY OF MATERIALS

pubs.acs.org/cm Article

B_2N_2-Doped Dibenzo[*a,m*]Rubicene: Modular Synthesis, Properties, and Coordination-Induced Color Tunability

Takumi Sakamaki, Takayuki Nakamuro, Keitaro Yamashita, Kunio Hirata, Rui Shang,* and Eiichi Nakamura*

Cite This: *Chem. Mater.* 2021, 33, 5337−5344 Read Online

ABSTRACT: B_2N_2-doped dibenzo[*a,m*]rubicene (**B_2N_2−DBR**) and derivatives possessing two B−N units C_{2h}-symmetrically on two edges are synthesized on a multigram scale via a two-step modular synthetic route using commercially available indole, aldehyde, and dichloroborane. Photophysical and electrochemical properties, crystal packing, and the reactivity of **B_2N_2−DBR** have been investigated. **B_2N_2−DBR** showed a larger optical gap and hence blue-shifted absorption and emission with a larger fluorescence quantum yield (Φ = 0.88) and a much smaller Stokes shift than its all-carbon analogue (**DBR**, Φ = 0.25). The blue-emissive **B_2N_2−DBR** derivatives are stable under ambient conditions against water and air but sensitive to nucleophiles such as fluoride and pyridine. **B_2N_2−DBR** reversibly interacts with a fluoride ion to bathochromically shift its emission with retention of a high fluorescence quantum yield, while coordination with pyridine quenches its photoluminescence. The marked changes in luminescence properties and optical gap on interaction with a Lewis base along with good chemical stability suggest the application of **B_2N_2−DBR** derivatives in colorimetric chemo- and biosensors.

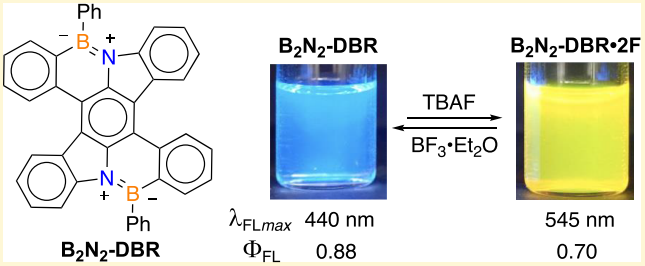

Emissive π-conjugated molecules with their photophysical properties tunable by external stimuli are valuable candidates for dopant-responsive organic electronic materials and colorimetric sensor applications.[1−18] For these compounds to be practically useful, they must be stable under ambient conditions against water and air, the quantum yield must be high, the color change must be significant, and they must be readily available on a large scale.[19,20] However, chemical responsiveness is often synonymous with instability as was observed that boron-doped aromatics with high acidity for sensing are susceptible to ambient air and moisture to protonate C−B bonds, thus requiring kinetic stabilization by steric protection.[21,22] Addition of nitrogen to boron-doped compounds creates more stable isoelectronically BN-doped compounds,[23,24] but they are less responsive to sensing—a trade-off between stability and responsiveness. We considered that an emissive benzo[1,2-*b*:4,5-*b*′]dipyrrole skeleton **A** connected to Lewis acidic boron substituents (**B**) provides a rational sensing mechanism through reversibly sequestering and releasing the nitrogen lone pair of pyrrole units (**C**, Figure 1a).[25−38] Apparently, **B** without stabilization is too structurally unstable (e.g., with respect to water hydrolysis) to be used as materials. We consider that B_2N_2-doped dibenzo[*a,m*]rubicene (**B_2N_2−DBR**, Figure 1b) presents a conjugated structure incorporating such a framework of **B**. We describe here the synthesis and properties of **B_2N_2−DBR**, where the framework **B** is stably embedded in a rigid dibenzo[*a,m*]rubicene skeleton (**DBR**, Figure 1c).[39,40]

The molecule shows blue fluorescence with a quantum yield Φ = 0.88, much higher than that of **DBR** (Φ = 0.25), and treatment with 2 equiv of fluoride ion results in a reversible color change from blue to yellow (545 nm, Φ = 0.70) with retention of a high fluorescence quantum yield (FLQY). The emission is quenched reversibly upon treatment with pyridine and recovered by treating with acidic water. With framework **B** embedded in the large planar π-network of **DBR**, **B_2N_2−DBR** is stable against moisture, acidic water, and heat up to 200 °C. The synthesis of **B_2N_2−DBR** and derivatives from indole, benzaldehyde, and dichlorophenylborane has been achieved using a two-pot procedure with the formation of eight covalent bonds in good overall yield on a multigram scale (Scheme 1).

Scheme 1 shows the two-pot modular synthetic route to **B_2N_2−DBR**. In the first step, 1 equiv each of an indole and a benzaldehyde was condensed in the presence of a catalytic amount of hydrogen iodide at room temperature followed by oxidative aromatization with iodine to obtain 6,12-diaryl-5,11-dihydroindolo[3,2-*b*]carbazoles (**DAIC**) in 40−68% isolated yields.[41] In the second step, treatment of **DAIC** with

Received: April 26, 2021
Revised: June 8, 2021
Published: June 16, 2021

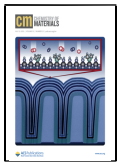

https://doi.org/10.1021/acs.chemmater.1c01441
Chem. Mater. 2021, 33, 5337−5344

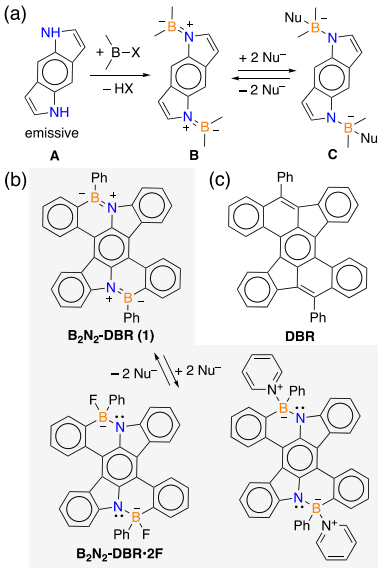

Figure 1. From benzo[1,2-*b*:4,5-*b*′]dipyrrole to **B$_2$N$_2$−DBR**. The structural representation of aromaticity is based on the graph theoretical analysis of **DBR**. (a) Sensing mechanism of N-boron-connected benzodipyrrole skeleton. Chemical structures of (b) **B$_2$N$_2$−DBR** and (c) **DBR**.

Scheme 1. Modular Synthesis of B$_2$N$_2$−DBR Derivatives

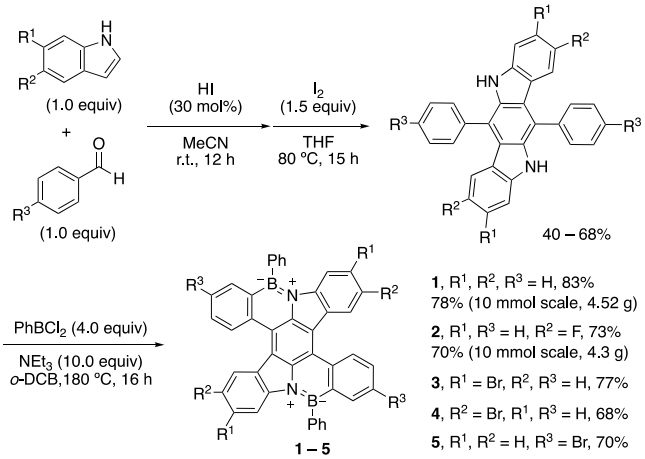

dichlorophenylborane at 180 °C produced **B$_2$N$_2$−DBR** (**1**−**5**) in 68−83% yields.[42−45] We prepared **1** and **2** on a multigram scale. We prepared halogenated derivatives **2**−**5** to examine the electronic tunability and further structural modifications via cross-coupling as discussed below (Scheme 2). These compounds are soluble in common organic solvents such as tetrahydrofuran (THF), dichloromethane (DCM), and toluene.

B$_2$N$_2$−DBR and derivatives are chemically robust compounds. Bromination with 2.5 equiv of bromine provided **3** in 52% yield after reprecipitation without affecting the B−N linkage.[46,47] The C−B bonds were tolerated under the conditions of Suzuki−Miyaura coupling and Sonogashira coupling, and we obtained diphenylated (**6**) and phenylethynylated (**7**) derivatives from dibromide **5**.[48−51] We prepared **6** and **7** for tuning of emission. The phenylethynyl group in **7** is known to increase the FLQY by enhancing the rate of radiative decay (k_r) relative to that of nonradiative

Scheme 2. Bromination, Suzuki−Miyaura Coupling, and Sonogashira Coupling on B$_2$N$_2$−DBR

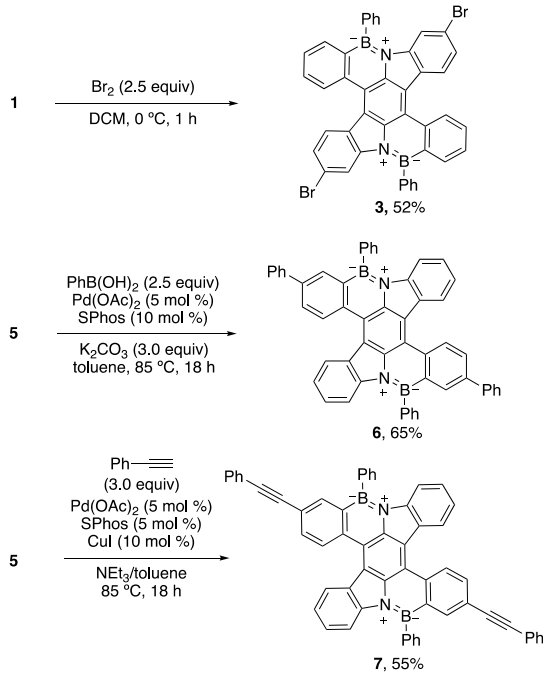

decay (k_{nr}).[52−56] All **B$_2$N$_2$−DBR** compounds (**1**−**7**) are stable in air and moisture.

A synchrotron X-ray crystallographic study provided the structure information of **1** as shown in Figure 2. Representative

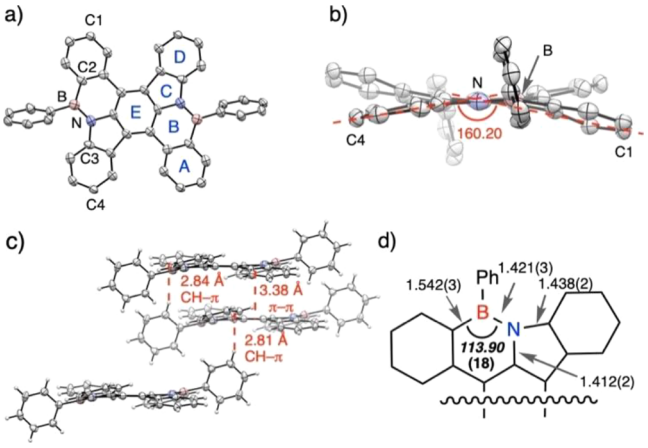

Figure 2. Crystal structure of **1**. (a) ORTEP drawing with thermal ellipsoids set to 50% probability. (b) Side view of **1**. (c) Packing structure of **1** in the crystal with intermolecular C−H−π and π−π interactions indicated in red color. (d) Representative synchrotron X-ray structural data (in Å and °; substituents are omitted) of **1**. Error ranges shown in parenthesis.

structural data of **1** are shown in Figure 2d. The B−N bond length of 1.421 Å reflects the double-bond character,[57−68] which is responsible for the nucleophilic addition of fluoride ion and pyridine discussed later. As in **DBR** (see Supporting Information for the crystal structure of **DBR**), **1** showed an achiral *anti*-folded polycyclic backbone with a folding angle of 160.2° connecting C1−N−C4 in the crystal lattice. The molecule packing of **1** is dominated by both edge-to-face C−H−π interaction and π−π interaction. The C−H−π

https://doi.org/10.1021/acs.chemmater.1c01441
Chem. Mater. 2021, 33, 5337−5344

interactions occur between the *meta*-C−H bond of the substituting phenyl with ring A and the *ortho*-C−H bond of the phenyl with ring D on the polycyclic backbone (Figure 2a,c). The $\pi-\pi$ interactions occur between the central benzene ring E and ring A (Figure 2a,c).

B_2N_2−DBR and **DBR** show substantially different spectral properties, reflecting the difference in their electronic structures, as shown in Figure 3a,b and Table 1. The

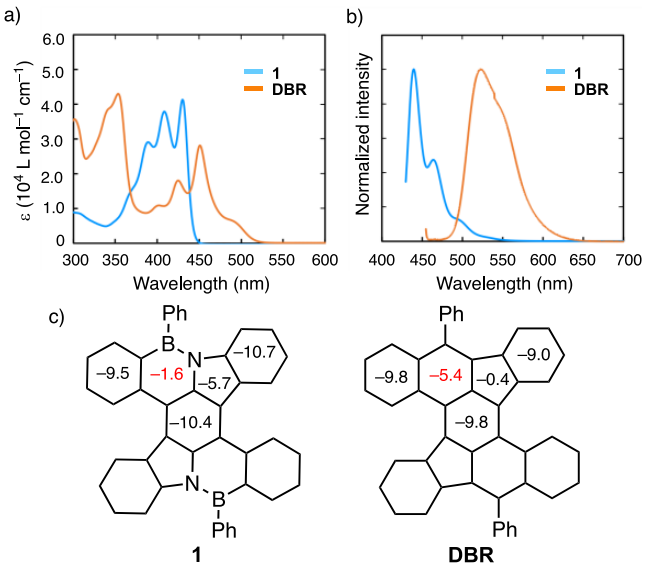

Figure 3. Comparison of the photophysical properties and aromaticity of **1** and **DBR**. (a) Absorption (1.0×10^{-5} M) and (b) emission (1.0×10^{-6} M) spectra of **1** and **DBR** in DCM. (c) NICS(1) values (in ppm) of **1** and **DBR** calculated at the GIAO-B3LYP/6-31G(d) level.

absorption maximum of **1** is blue-shifted by 21 nm relative to that of **DBR**. The optical gap estimated from the absorption onset of **1** (2.79 eV) is much larger than that of **DBR** (2.47 eV), which is consistent with the density functional theory calculation (see Supporting Information for details). **B_2N_2−DBR** emits blue fluorescence in DCM with an emission maximum at 440 nm with a smaller peak at 462 nm. The 0.88 FLQY of **1** is much larger than the 0.25 FLQY of **DBR**. The high FLQY is attributed to molecular rigidity and the increased transition probability that enhance the radiative decay rate by inclusion of ionic B−N units that shift the orbital symmetry. We found that the FLQY of **1** in the solid state remains at a rather high value of 0.29.

Nucleus-independent chemical shift NICS(1) calculations were performed at the GIAO-B3LYP/6-31G(d) level to compare **1** and **DBR** for their electronic structures and aromaticities.[69] As shown in Figure 3c, the azaborine ring in **1** shows an NICS(1) value of −1.6 ppm (nonaromatic), while the corresponding ring in **DBR** is clearly aromatic (−5.4 ppm). The difference in electronegativity between boron and nitrogen induces an ionic character, which leads to increased localization of electrons on the B−N units, resulting in poor aromaticity. On the other hand, the lone pair localized on nitrogen satisfies Hückel's rule for the carbazole ring, leading to higher aromaticity than the corresponding five-membered carbon ring in **DBR**. NICS values indicate that the five-membered carbazole ring system in **1** is aromatic, while the corresponding five-membered carbon ring in **DBR** is expectedly nonaromatic.

B_2N_2−DBR has a higher highest occupied molecular orbital (HOMO) level than **DBR**. Photoelectron yield spectroscopy (PYS)[70] measurement of a film deposited on an ITO substrate showed ionization potentials (IPs) of 5.35 eV for **1** and 5.83 eV for **DBR** (Table 2). Cyclic voltammetry measurement in

Table 2. Electrochemical Properties of 1 and DBR

	IP (eV)[a]	E_{ox} (V vs Fc/Fc$^+$)[b]	OBG (eV)[c]	E_H (eV)[d]	E_L (eV)[e]
1	5.35	0.95, 1.26	2.79	−5.75	−2.96
DBR	5.83	1.19	2.47	−5.99	−3.52

[a]IP measured using PYS for a film deposited on an ITO surface. [b]Oxidation potential (0.5 mM DCM with 0.1 M Bu_4NPF_6 electrolyte). [c]Optical gap determined from the offset of the absorption spectra. [d]HOMO level determined from the oxidation potential. [e]LUMO level determined from the oxidation potential and optical gap.

DCM showed that the first oxidation potential of **1** was 0.95 V versus Fc/Fc$^+$, while that of **DBR** was 1.19 V versus Fc/Fc$^+$. Unlike **DBR**, **1** undergoes two irreversible oxidations at 0.95 and 1.26 V versus Fc/Fc$^+$. HOMO levels determined from the first oxidation potentials of **1** and **DBR** are −5.75 and −5.99 eV, respectively, values expected from the IP data in the solid state. The LUMO level of **1** (−2.96 eV) was much higher than that of **DBR** (−3.52 eV) calculated from the higher HOMO and larger optical gap of **1**.

Table 3 summarizes the photophysical properties of **6** and **7**. The bis-phenylated (**6**) and bis-phenylethynylated (**7**) **B_2N_2−**

Table 3. Photophysical Properties of 6 and 7

	λ_{abs} (nm)[a]	λ_{FL} (nm)[b]	Stokes shift (nm)	Φ_{FL}[c]	τ_{FL} (ns)[d]	k_r (10^8 s^{-1})	k_{nr} (10^8 s^{-1})
6	400, 425, 450	458, 484	8	0.80	2.45	3.3	0.82
7	412, 430, 457	470, 497	13	0.81	2.03	4.0	0.93

[a]Absorption (λ_{abs}) maxima measured in DCM. [b]Fluorescence maxima (λ_{FL}) measured in DCM. [c]FLQY in solution determined using an absolute method. [d]Fluorescence lifetime measured in the time-correlated single-photon counting operation mode.

Table 1. Photophysical Properties of 1 and DBR

	λ_{abs} (nm)[a]	λ_{FL} (nm)[b]	Stokes shift (nm)	Φ_{FL}[c]	τ_{FL} (ns)[d]	k_r (10^8 s^{-1})	k_{nr} (10^8 s^{-1})
1	389, 408, 430	440, 462	10	0.88 (0.29)	4.40	2.0	0.27
DBR	355, 425, 451	523	72	0.25	6.38	0.39	1.17

[a]Absorption (λ_{abs}) maxima measured in DCM. [b]Fluorescence maxima (λ_{FL}) measured in DCM. [c]FLQY in solution determined using an absolute method. Solid-state FLQY values in parentheses. [d]Fluorescence lifetime measured in the time-correlated single-photon counting operation mode.

https://doi.org/10.1021/acs.chemmater.1c01441
Chem. Mater. 2021, 33, 5337−5344

DBR showed maximum absorption peaks red-shifted by 20 and 27 nm compared with that of **1** because of the extended conjugation. Both **6** and **7** luminesce intensely with quantum yields of 0.80 and 0.81 and fluorescence lifetimes of τ_{FL} = 2.45 ns and τ_{FL} = 2.03 ns, respectively. The increased k_r values of **6** and **7** compared to **1** can be explained by their increased absorption coefficients as observed in their UV−vis spectra (see Supporting Information S16 for details).

Finally, we describe fluorescence switching by coordination of fluoride ion and pyridine (see below). The addition of a THF solution of tetrabutylammonium fluoride (TBAF) to a DCM solution of **1** resulted in dramatic changes in the color of absorption and emission due to the formation of an anionic fluoride adduct. The adduct formation breaks the conjugation and sharply changes the electronic properties of boron atoms. The absorption red-shifted as much as 94 nm from 430 to 524 nm and the emission from 440 (blue) to 545 nm (yellow) with an FLQY of 0.70 (Figure 4a,b). Chloride ion and bromide ion did not affect the color because of smaller bond energies of B−Cl and B−Br than B−F. The redshift stands in contrast to the blueshift normally observed for boron-containing aromatics interacting with fluoride ion, which hampers pπ−π* conjugation.[1,71,72]

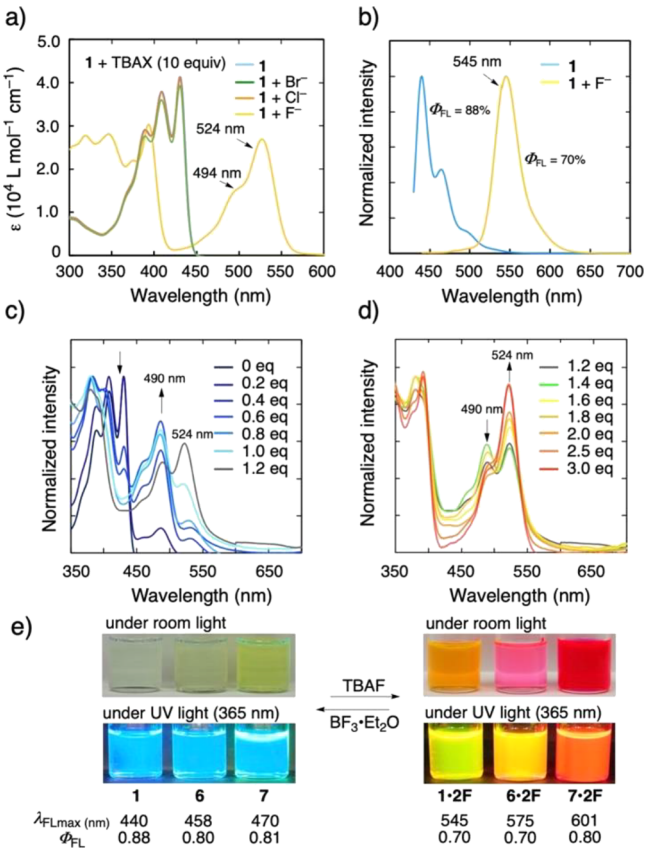

Figure 4. Effect of fluoride ion coordination on photophysical properties of B_2N_2−**DBR** and analogues. (a) Effect of halogen ion coordination to **1** on absorption. The UV−vis spectra was recorded by adding a solution of tetrabutylammonium salt (10 equiv) in THF to a solution of **1** in DCM (1.0×10^{-4} M). (b) Fluorescence spectra (1.0×10^{-6} M) and quantum yields of **1** and **1•2F**. (c,d) Spectroscopic titration of **1** with TBAF. (e) Reversible change of visual color and photophysical properties of B_2N_2−**DBR** and analogues (**1**, **6**, and **7**) upon fluoride ion coordination.

UV−vis spectral titration with TBAF showed that a new absorption peak at 490 nm maximizes at nearly a 1:1 ratio, and this peak was assigned to a monofluoride adduct (Figure 4c). Upon further addition of TBAF, a band at 524 nm increased at a 1:2 ratio, reaching a plateau at a 1:2.5 ratio. We therefore conclude that the spectral change is due to the formation of **1•2F** (Figure 4d). The phenyl analogue **6** and phenylethynyl analogue **7** showed similar behaviors. Upon addition of excess fluoride ions, both **6** and **7** luminesce intensely with FLQYs of 0.70 and 0.80, respectively. The emission maxima were red-shifted from 458 to 575 nm for **6** and from 470 to 601 nm for **7**, red-shifted by 117 and 131 nm, respectively (see Supporting Information for details on UV−vis absorption and emission spectra). Notably, addition of an excess of BF_3•Et_2O reverted both absorption and emission to normal, indicating that the fluoride coordination is reversible (Figure 4e).

In pyridine, **1** shows strong solvatochromism and fluorescence quenching. Upon dissolution in pyridine, three new absorption peaks at 492, 467, and 320 nm emerged (Figure 5a), and the fluorescence was quenched almost entirely

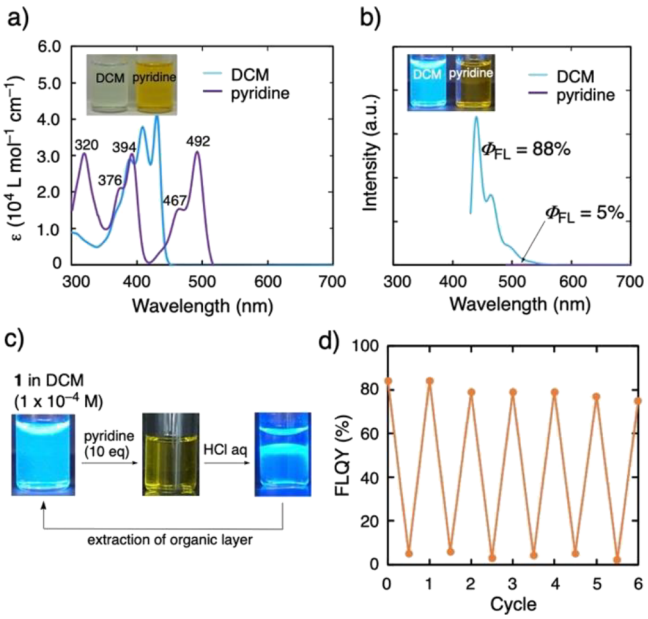

Figure 5. Effect of pyridine coordination on photophysical properties. (a) Absorption spectra recorded in DCM and in pyridine (1.0×10^{-5} M). (b) Fluorescence spectra (1.0×10^{-6} M) upon pyridine coordination. (c) Recovery of fluorescence upon adding HCl. (d) Repetitive fluorescence quenching and recovery by treatment with pyridine and HCl.

(Figure 5b), suggesting the formation of an adduct between **1** and two pyridine molecules.[73−77] The fluorescence quenching with pyridine is reversible, and **1** is stable in aqueous hydrochloric acid (HCl) as indicated by the 6 cycles of the quenching/recovery experiment shown in Figure 5c,d using pyridine and HCl.

A comparison of the frontier molecular orbital (FMO) properties and the calculated geometries of **1** and **1•2F** provides a rationale for the observed effects of donor coordination.[78,79] As shown in Figure 6, the calculated HOMO level of −5.67 eV and the HOMO−LUMO gap of 3.36 eV agree favorably with the experimental IP and oxidation potential data (5.35 and −5.75 eV, see above) and the optical gap of 2.79 eV. According to the results of time-dependent

https://doi.org/10.1021/acs.chemmater.1c01441
Chem. Mater. 2021, 33, 5337−5344

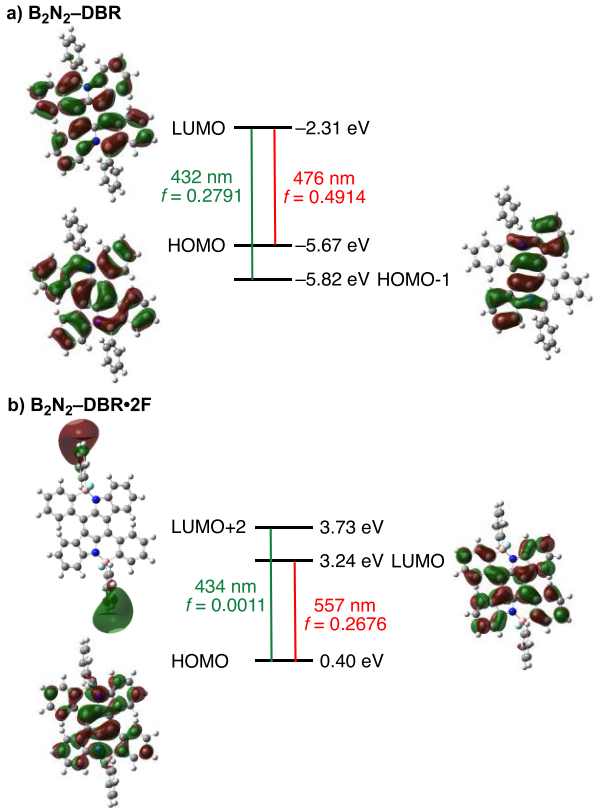

Figure 6. FMO orbitals and energies of **1** and **1•2F**. Comparison of molecular orbital energetics of **1** (a) and fluoride ion adduct **1•2F** (b) using TD-DFT calculations at the B3LYP/6-31 + G(d, p) level of theory.

density functional theory (TD-DFT) calculations, the first absorption peak of **1** is due to the transition between HOMO and LUMO. The fluoride ion coordination pushes up the HOMO level by 6.07 eV and narrows the bandgap to 2.84 eV, coinciding with the large experimental bathochromic shift of absorption and emission. Transition of natural orbitals involved in the first absorption and emission of **1•2F** is the HOMO−LUMO transition. **1** shows a delocalized HOMO and LUMO encompassing the whole aromatic core, which greatly changes upon fluoride ion coordination. The calculated B−N bond length of 1.44 Å (experimental value, 1.42 Å; see Figure 2) becomes 1.56 Å upon fluoride ion coordination as a result of the release of the nitrogen lone pair from boron. In the case of pyridine coordination, the length of the B−N bond becomes 1.53 Å.

In summary, we have presented a new design for an emissive molecule for fluorescence switching by doping a benzo[1,2-*b*:4,5-*b*′]dipyrrole skeleton as part of a **B_2N_2−DBR** skeleton. The two-pot synthesis relying on a robust synthetic scheme is efficient in making eight new bonds from readily available indole, benzaldehyde, and dichlorophenylborane, affording **B_2N_2−DBR** on a multigram scale. The parent compound and its derivatives show blue fluorescence with FLQY of 0.80−0.88, and they are air-, water-, and heat-stable, surviving treatment with fluoride ion, BF_3•Et_2O, pyridine, and acidic water. Treatment of the blue-emitting phenylethynyl derivative **7** with fluoride ion redshifts the blue fluorescence as much as 131 nm, emitting at 601 nm (orange) with an FLQY of 0.80. Pyridine, on the other hand, quenches the emission. The observed stability and the fluorescence switching with a Lewis base suggest their application in colorimetric chemo- and biosensors.[80−84]

■ EXPERIMENTAL SECTION

General Procedure. All the reactions dealing with air- or moisture-sensitive compounds were carried out in a dry reaction vessel under a positive pressure of nitrogen. Air- and moisture-sensitive liquids and solutions were transferred via a syringe or a Teflon cannula. Analytical thin-layer chromatography (TLC) was performed using glass plates precoated with 0.25 mm, 230−400 mesh silica gel impregnated with a fluorescent indicator (254 nm). TLC plates were visualized by exposure to ultraviolet light. Flash column chromatography was performed as described by Still et al.,[85] employing a Kanto Silica gel 60 (spherical, neutral, 140−325 mesh). Unless otherwise stated, commercial reagents were purchased from Tokyo Kasei Co., Aldrich Inc., and other commercial suppliers and used as purchased. Anhydrous solvents were purchased from Kanto and purified using a solvent purification system (Glass Contour) equipped with columns of activated alumina and a copper catalyst prior to use.

Multigram Scale Synthesis of B_2N_2−DBR. A mixture of **DAIC** (10 mmol) and triethylamine (100 mmol) in *o*-dichlorobenzene (100 mL) was stirred at room temperature for 10 min. Then, dichlorophenyl borane (40 mmol) was dropwise added to the reaction mixture. After stirring at room temperature for 15 min, the reaction mixture was heated up to 180 °C for 12 h. After cooling to room temperature, toluene was added to the reaction mixture. The insoluble moieties were removed by filtration. After removal of the solvent in vacuo, the solid was washed with ethyl acetate and collected by filtration. The obtained solid was sonicated with isopropyl alcohol and collected by filtration to give **B_2N_2−DBR**.

■ ASSOCIATED CONTENT

Supporting Information

The Supporting Information is available free of charge at https://pubs.acs.org/doi/10.1021/acs.chemmater.1c01441.

Synthesis of BN-doped dibenzorubicene and its congeners, crystallographic study, computational study, UV−vis absorption and fluorescence spectra, electrochemical studies, thermal studies, IP, and NMR spectra of the compounds (PDF)

Crystallographic data of DBR (CIF)

Crystallographic data of B_2N_2−DBR (CIF)

■ AUTHOR INFORMATION

Corresponding Authors

Rui Shang − *Department of Chemistry, The University of Tokyo, Tokyo 113-0033, Japan;* orcid.org/0000-0002-2513-2064; Email: rui@chem.s.u-tokyo.ac.jp

Eiichi Nakamura − *Department of Chemistry, The University of Tokyo, Tokyo 113-0033, Japan;* orcid.org/0000-0002-4192-1741; Email: nakamura@chem.s.u-tokyo.ac.jp

Authors

Takumi Sakamaki − *Department of Chemistry, The University of Tokyo, Tokyo 113-0033, Japan*

Takayuki Nakamuro − *Department of Chemistry, The University of Tokyo, Tokyo 113-0033, Japan;* orcid.org/0000-0002-0752-3475

Keitaro Yamashita − *Department of Biological Sciences, Graduate School of Science, The University of Tokyo, Tokyo 113-0033, Japan;* Present Address: MRC Laboratory of Molecular Biology, Francis Crick Avenue, Cambridge CB2 0QH, United Kingdom (K.Y.).

Kunio Hirata − *RIKEN/SPring-8 Center, Sayo-gun, Hyogo 679-5148, Japan*

Complete contact information is available at:
https://pubs.acs.org/10.1021/acs.chemmater.1c01441

Notes

The authors declare no competing financial interest.

■ ACKNOWLEDGMENTS

We thank JSPS for financial support (KAKENHI Grant-in-Aid for Scientific Research JP19H05459 to E.N. and JP19K15555 to R.S.). T.S. thanks JSPS for the MERIT program.

■ REFERENCES

(1) Yamaguchi, S.; Akiyama, S.; Tamao, K. Colorimetric Fluoride Ion Sensing by Boron-Containing π-Electron Systems. *J. Am. Chem. Soc.* **2001**, *123*, 11372−11375.

(2) Gal braith, E.; James, T. D. Boron based anion receptor as sensors. *Chem. Soc. Rev.* **2010**, *39*, 3831−3842.

(3) Jakle, F. Advances in the Synthesis of Organoborane Polymers for Optical, Electronic and Sensory Applications. *Chem. Rev.* **2010**, *110*, 3985−4022.

(4) Mellerup, S. K.; Wang, S. Boron-based stimuli responsive materials. *Chem. Soc. Rev.* **2019**, *48*, 3537−3549.

(5) Chi, Z.; Zhang, X.; Xu, B.; Zhou, X.; Ma, C.; Zhang, Y.; Liu, S.; Xu, J. Recent advances in organic mechanofluorochromic materials. *Chem. Soc. Rev.* **2012**, *41*, 3878−3896.

(6) Li, B.; Seth, K.; Niu, B.; Pan, L.; Yang, H.; Ge, H. Transient-Ligand-Enabled ortho-Arylation of Five-Membered Heterocycles: Facile Access to Mechanochromic Materials. *Angew. Chem., Int. Ed.* **2018**, *57*, 3401−3405.

(7) Isayama, K.; Aizawa, N.; Kim, J. Y.; Yasuda, T. Modulating Photo- and Electroluminescence in a Stimuli-Responsive π-Conjugated Donor−Acceptor Molecular System. *Angew. Chem., Int. Ed.* **2018**, *57*, 11982−11986.

(8) Liu, Y.; Zhou, J.; Wang, L. L.; Hu, X. X.; Liu, X. J.; Liu, M. R.; Cao, Z. H.; Shangguan, D. H.; Tan, W. H. A Cyanine Dye to Probe Mitophagy: Simultaneous Detection of Mitochondria and Autolysosomes in Live Cells. *J. Am. Chem. Soc.* **2016**, *138*, 12368−12374.

(9) Sun, S.; Ning, X.; Zhang, G.; Wang, Y. C.; Peng, C.; Zheng, J. Dimerization of Organic Dyes on Luminescent Gold Nanoparticles for Ratiometric pH Sensing. *Angew. Chem., Int. Ed.* **2016**, *55*, 2421−2424.

(10) Zuo, Y.; Wang, X.; Wu, D. Uniting aggregation-induced emission and stimuli-responsive aggregation-caused quenching, single molecule achieved multicolour luminescence. *J. Mater. Chem. C* **2019**, *7*, 14555−14562.

(11) Kim, J. H.; Jung, Y.; Lee, D.; Jang, W. D. Thermoresponsive Polymer and Fluorescent Dye Hybrids for Tunable Multicolor Emission. *Adv. Mater.* **2016**, *28*, 3499−3503.

(12) Chen, J. F.; Yin, X.; Wang, B.; Zhang, K.; Meng, G.; Zhang, S.; Shi, Y.; Wang, N.; Wang, S.; Chen, P. Planar Chiral Organoboranes with Thermoresponsive Emission and Circularly Polarized Luminescence: Integration of Pillar[5]arenes with Boron Chemistry. *Angew. Chem., Int. Ed.* **2020**, *59*, 11267−11272.

(13) Zhou, Y.; Zhang, J. F.; Yoon, J. Fluorescence and Colorimetric Chemosensors for Fluoride-Ion Detection. *Chem. Rev.* **2014**, *114*, 5511−5571.

(14) Ji, L.; Griesbeck, S.; Marder, T. B. Recent developments in and perspectives on three-coordinate boron materials: a bright future. *Chem. Sci.* **2017**, *8*, 846−863.

(15) Liu, Y.; Li, A.; Xu, S.; Xu, W.; Liu, Y.; Tian, W.; Xu, B. Reversible Luminescent Switching in an Organic Cocrystal: Multi-Stimuli-Induced Crystal-to-Crystal Phase Transformation. *Angew. Chem., Int. Ed.* **2020**, *59*, 15098−15103.

(16) Griesbeck, S.; Michail, E.; Wang, C.; Ogasawara, H.; Lorenzen, S.; Gerstner, L.; Zhang, T.; Nitsch, J.; Sato, Y.; Bertermann, R.; Taki, M.; Lambert, C.; Yamaguchi, S.; Marder, T. B. Tuning the π-Bridge of Quadrupolar Triarylborane Chromophores for One- and Two-Photon Excited Fluorescence Imaging of Lysosomes in Live Cells. *Chem. Sci.* **2019**, *10*, 5405−5422.

(17) Griesbeck, S.; Michail, E.; Rauch, F.; Ogasawara, H.; Wang, C.; Sato, Y.; Edkins, R.; Zhang, Z.; Taki, M.; Lambert, C.; Yamaguchi, S.; Marder, T. B. The Effect of Branching on One- and Two-Photon Absorption, Cell Viability and Localization of Cationic Triarylborane Chromophores with Dipolar vs. Octupolar Charge Distributions for Cellular Imaging. *Chem. − Eur. J.* **2019**, *25*, 13164−13175.

(18) Ferger, M.; Ban, Ž.; Krošl, I.; Tomić, S.; Dietrich, L.; Lorenzen, S.; Rauch, F.; Sieh, D.; Friedrich, A.; Griesbeck, S.; Kenđel, A.; Miljanić, S.; Piantanida, I.; Marder, T. B. Bis(phenylethynyl)arene Linkers in Tetracationic bis-Triarylborane Chromophores Control Fluorimetric and Raman Sensing of Various DNA and RNA. *Chem. − Eur. J.* **2021**, *27*, 5142−5159.

(19) Entwistle, C. D.; Marder, T. B. Boron Chemistry Lights the Way: Optical Properties of Molecular and Polymeric Systems. *Angew. Chem., Int. Ed.* **2002**, *114*, 3051−3056.

(20) Entwistle, C. D.; Marder, T. B. Applications of Three-Coordinate Organoboron Compounds and Polymers in Optoelectronics. *Chem. Mater.* **2004**, *16*, 4574−4585.

(21) Rachel, J. K.; Wisit, H.; Jessica, C.; Michael, J. I.; Robert, A. W. D. Well-Defined Boron/Nitrogen-Doped Polycyclic Aromatic Hydrocarbons Are Active Electrocatalysts for the Oxygen Reduction Reaction. *Chem. Mater.* **2019**, *31*, 1891−1898.

(22) Su, X.; Bartholome, T. A.; Tidwell, J. R.; Pujol, A.; Yruegas, S.; Martinez, J. J.; Martin, C. D. 9-Borafluorenes: Synthesis, Properties, and Reactivity. *Chem. Rev.* **2021**, *121*, 4147−4192.

(23) Liu, Z.; Marder, T. B. B−N versus C−C: How Similar Are They? *Angew. Chem., Int. Ed.* **2008**, *47*, 242−244.

(24) Bosdet, M. J. D.; Piers, W. E. BN as a CC substitute in aromatic systems. *Can. J. Chem.* **2009**, *87*, 8−29.

(25) Tsuji, H.; Yokoi, Y.; Furukawa, S.; Nakamura, E. Hexaarylbenzodipyrroles: Properties and Application as Amorphous Carrier-Transporting Materials. *Heterocycles* **2015**, *90*, 261−270.

(26) Tsuji, H.; Yokoi, Y.; Mitsui, C.; Ilies, L.; Sato, Y.; Nakamura, E. Tetraaryl-substituted Benzo[1,2-*b*:4,5-*b*′]dipyrroles: Synthesis, Properties, and Applications to Hole-injection Materials in OLED Devices. *Chem. − Asian J.* **2009**, *4*, 655−657.

(27) Shang, R.; Zhou, Z.; Nishioka, H.; Halim, H.; Furukawa, S.; Takei, I.; Ninomiya, N.; Nakamura, E. Disodium Benzodipyrrole Sulfonate as Neutral Hole-Transporting Materials for Perovskite Solar Cells. *J. Am. Chem. Soc.* **2018**, *140*, 5018−5022.

(28) Zhou, Z.; Qiang, Z.; Sakamaki, T.; Takei, I.; Shang, R.; Nakamura, E. Organic/Inorganic Hybrid p-Type Semiconductor Doping Affords Hole-Transporting-Layer-Free Thin-film Perovskite Solar Cells with High Stability. *ACS Appl. Mater. Interfaces* **2019**, *11*, 22603−22611.

(29) Reus, C.; Weidlich, S.; Bolte, M.; Lerner, H. W.; Wagner, M. C-Functionalized, Air- and Water-Stable 9,10-Dihydro-9,10-diboraanthracenes: Efficient Blue to Red Emitting Luminophores. *J. Am. Chem. Soc.* **2013**, *135*, 12892−12907.

(30) Aude, E.; Michael, J. I. Fused polycyclic aromatics incorporating boron in the core: fundamentals and applications. *Chem. Commun.* **2015**, *51*, 6257−6274.

(31) Schickedanz, K.; Radtke, J.; Bolte, M.; Lerner, H. W.; Wagner, M. Facile Route to Quadruply Annulated Borepins. *J. Am. Chem. Soc.* **2017**, *139*, 2842−2851.

(32) Liu, K.; Lalancette, R. A.; Jäkle, F. B−N Lewis Pair Functionalization of Anthracene: Structural Dynamics, Optoelectronic Properties, and O_2 Sensitization. *J. Am. Chem. Soc.* **2017**, *139*, 18170−18173.

(33) Li, S. Y.; Sun, Z. B.; Zhao, C. H. Charge-Transfer Emitting Triarylborane π-Electron Systems. *Inorg. Chem.* **2017**, *56*, 8705−8717.

(34) Scholz, A. S.; Massoth, J. G.; Bursch, M.; Mewes, J. M.; Hetzke, T.; Wolf, B.; Bolte, M.; Lerner, H. W.; Grimme, S.; Wagner, M. BNB-Doped Phenalenyls: Modular Synthesis, Optoelectronic Properties,

and One-Electron Reduction. *J. Am. Chem. Soc.* **2020**, *142*, 11072−11083.
(35) Suresh, S. M.; Hall, D.; Beljonne, D.; Olivier, Y.; Zysman-Colman, E. Multiresonant thermally activated delayed fluorescence emitters based on heteroatom-doped nanographenes: Recent advances and prospects for organic light-emitting diodes. *Adv. Funct. Mater.* **2020**, *30*, No. 1908677.
(36) Zhao, C. H.; Sakuda, E.; Wakamiya, A.; Yamaguchi, S. Highly Emissive Diborylphenylene−Containing Bis(phenylethynyl)benzenes: Structure−Photophysical Property Correlations and Fluoride Ion Sensing. *Chem. − Eur. J.* **2009**, *15*, 10603−10612.
(37) Grotthuss, E. V.; John, A.; Kaese, T.; Wagner, M. Doping Polycyclic Aromatics with Boron for Superior Performance in Materials Science and Catalysis. *Asian J. Org. Chem.* **2018**, *7*, 37−53.
(38) He, J.; Rauch, F.; Friedrich, A.; Krebs, J.; Krummenacher, I.; Bertermann, R.; Nitsch, J.; Braunschweig, H.; Finze, M.; Marder, T. B. Phenylpyridyl-Fused Boroles: A Unique Coordination Mode and Weak B−N Coordination-Induced Dual Fluorescence. *Angew. Chem., Int. Ed.* **2021**, *60*, 4833−4840.
(39) For dibenzo[*a,m*]rubicenes, see; Gu, X.; Xu, X.; Li, H.; Liu, Z.; Miao, Q. Synthesis, Molecular Packing, and Thin Film Transistors of Dibenzo[*a,m*]rubicenes. *J. Am. Chem. Soc.* **2015**, *137*, 16203−16208.
(40) For nitrogen-doped rubicene, see: Park, Y. S.; Dibble, D. J.; Kim, J.; Lopez, R. C.; Vargas, E.; Gorodetsky, A. A. Synthesis of Nitrogen-Containing Rubicene and Tetrabenzopentacene Derivatives. *Angew. Chem., Int. Ed.* **2016**, *55*, 3352−3355.
(41) Gu, R.; Snick, S. V.; Robeyns, K.; Meervelt, L. V.; Dehaen, W. A facile and general method for the synthesis of 6,12-diaryl-5,11-dihydroindolo[3,2-*b*]carbazoles. *Org. Biomol. Chem.* **2009**, *7*, 380−385.
(42) Hatakeyama, T.; Hashimoto, S.; Seki, S.; Nakamura, M. Synthesis of BN-Fused Polycyclic Aromatics via Tandem Intramolecular Electrophilic Arene Borylation. *J. Am. Chem. Soc.* **2011**, *133*, 18614−18617.
(43) Campbell, P. G.; Marwitz, A. J. V.; Liu, S. Y. Recent Advances in Azaborine Chemistry. *Angew. Chem., Int. Ed.* **2012**, *51*, 6074−6092.
(44) Wang, X. Y.; Zhuang, F. D.; Wang, R. B.; Wang, X. C.; Cao, X. Y.; Wang, J. Y.; Pei, J. A Straightforward Strategy toward Large BN-Embedded π-Systems: Synthesis, Structure, and Optoelectronic Properties of Extended BN Heterosuperbenzenes. *J. Am. Chem. Soc.* **2014**, *136*, 3764−3767.
(45) Wang, X. Y.; Wang, J. Y.; Pei, J. BN Heterosuperbenzenes: Synthesis and Properties. *Chem. − Eur. J.* **2015**, *21*, 3528−3539.
(46) Huang, H.; Zhou, Y.; Wang, M.; Zhang, J.; Cao, X.; Wang, S.; Cao, D.; Cui, C. Regioselective Functionalization of Stable BN-Modified Luminescent Tetraphenes for High-Resolution Fingerprint Imaging. *Angew. Chem., Int. Ed.* **2019**, *58*, 10132−10137.
(47) Zhang, C.; Zhang, L.; Sun, C.; Sun, W.; Liu, X. BN-Phenanthrenes: Synthesis, Reactivity, and Optical Properties. *Org. Lett.* **2019**, *21*, 3476−3480.
(48) Corbet, J.; Mignani, G. Selected Patented Cross-Coupling Reaction Technologies. *Chem. Rev.* **2006**, *106*, 2651−2710.
(49) Jana, R.; Pathak, T. P.; Sigman, M. S. Advances in Transition Metal (Pd,Ni,Fe)-Catalyzed Cross-Coupling Reactions Using Alkyl-organometallics as Reaction Partners. *Chem. Rev.* **2011**, *111*, 1417−1492.
(50) Giustra, Z. X.; Liu, S. Y. The State of the Art in Azaborine Chemistry: New Synthetic Methods and Applications. *J. Am. Chem. Soc.* **2018**, *140*, 1184−1194.
(51) McConnell, C. R.; Liu, S. Y. Late-stage functionalization of BN-heterocycles. *Chem. Soc. Rev.* **2019**, *48*, 3436−3453.
(52) Nguyen, P.; Todd, S.; Biggelaar, V. D. D.; Taylor, N. J.; Marder, T. B.; Wittmann, F.; Friend, R. H. Facile Route to Highly Fluorescent 9,10-Bis(p-R-phenylethynyl)anthracene Chromophores via Palladium/Copper Catalyzed Cross-Coupling. *Synlett* **1994**, *4*, 299−301.
(53) Maeda, H.; Maeda, T.; Mizuno, K.; Fujimoto, K.; Shimizu, H.; Inouye, M. Alkynylpyrenes as Improved Pyrene-Based Biomolecular Probes with the Advantages of High Fluorescence Quantum Yields and Long Absorption/ Emission Wavelengths. *Chem. − Eur. J.* **2006**, *12*, 824−831.
(54) Crawford, A. G.; Dwyer, A. D.; Liu, Z.; Steffen, A.; Beeby, A.; Pålsson, L. O.; Tozer, D. J.; Marder, T. B. Experimental and Theoretical Studies of the Photophysical Properties of 2- and 2,7-Functionalized Pyrene Derivatives. *J. Am. Chem. Soc.* **2011**, *133*, 13349−13362.
(55) Hakoda, Y.; Aoyagi, M.; Irisawa, K.; Kato, S.; Nakamura, Y.; Yamaji, M. Photochemical synthesis and photophysical features of ethynylphenanthrenes studied by emission and transient absorption measurements. *Photochem. Photobiol. Sci.* **2016**, *15*, 1586−1593.
(56) Lübtow, M.; Helmers, I.; Stepanenko, V.; Albuquerque, R. Q.; Marder, T. B.; Fernandez, G. Self-Assembly of 9,10-Bis-(phenylethynyl)anthracene (BPEA) Derivatives: Influence of $\pi-\pi$ and Hydrogen Bonding Interactions on Aggregate Morphology and Self-Assembly Mechanism. *Chem. − Eur. J.* **2017**, *23*, 6198−6205.
(57) Dewar, M. J. S.; Kubba, V. P.; Pettit, R. J. New heteroaromatic compounds. Part I. 9-Aza-10-boraphenanthrene. *J. Chem. Soc.* **1958**, 3073−3076.
(58) Dewar, M. J. S.; Kaneko, C.; Bhattacharjee, M. K. New Heteroaromatic Compounds. XVI. Compounds with Heteroatoms at Bridgeheads. *J. Am. Chem. Soc.* **1962**, *84*, 4884−4887.
(59) Culling, G. C.; Dewar, M. J. S.; Marr, P. A. New Heteroaromatic Compounds. XXIII. Two Analogs of Triphenylene and a Possible Route to Borazarene. *J. Am. Chem. Soc.* **1964**, *86*, 1125−1127.
(60) Davies, K. M.; Dewar, M. J. S.; Rona, P. New heteroaromatic compounds. XXVI. Synthesis of borazarenes. *J. Am. Chem. Soc.* **1967**, *89*, 6294−6297.
(61) Sorensen, W. E.; Parvez, T. S. M. Triphenylene Analogues with $B_2N_2C_2$ Cores: Synthesis, Structure, Redox Behavior, and Photophysical Properties. *J. Am. Chem. Soc.* **2006**, *128*, 10885−10896.
(62) Bosdet, M. J. D.; Jaska, C. A.; Piers, W. E.; Sorensen, T. S.; Parvez, M. Blue Fluorescent 4*a*-Aza-4*b*-boraphenanthrenes. *Org. Lett.* **2007**, *9*, 1395−1398.
(63) Bosdet, M. J. D.; Piers, W. E.; Sorensen, T. S.; Parvez, M. 10-Aza-10*b*-borapyrenes: Heterocyclic Analogues of Pyrene with Internalized BN Moieties. *Angew. Chem., Int. Ed.* **2007**, *46*, 4940−4943.
(64) Ashe, A. J.; Fang, X. A Synthesis of Aromatic Five- and Six-Membered B−N Heterocycles via Ring Closing Metathesis. *Org. Lett.* **2000**, *2*, 2089−2091.
(65) Ashe, A. J.; Fang, X.; Fang, X.; Kampf, J. W. Synthesis of 1,2-Dihydro-1,2-azaborines and Their Conversion to Tricarbonyl Chromium and Molybdenum Complexes. *Organometallics* **2001**, *20*, 5413−5418.
(66) Pan, J.; Kampf, J. W.; Ashe, A. J. 1,2-Azaboratabenzene: A Heterocyclic π-Ligand with an Adjustable Basicity at Nitrogen. *Organometallics* **2004**, *23*, 5626−5629.
(67) Fang, X.; Yang, H.; Kampf, J. W.; Holl, M. M. B.; Ashe, A. J. Syntheses of Ring-Fused B−N Heteroaromatic Compounds. *Organometallics* **2006**, *25*, 513−518.
(68) Pan, J.; Kampf, J. W.; Ashe, A. J. Electrophilic Aromatic Substitution Reactions of 1,2-Dihydro-1,2-azaborines. *Org. Lett.* **2007**, *9*, 679−681.
(69) Shaidaei, H. F. B.; Wannere, C. S.; Corminboeuf, C.; Puchta, R.; Schleyer, P. v. R. Which NICS Aromaticity Index for Planar π Rings Is Best? *Org. Lett.* **2006**, *8*, 863−866.
(70) Lacher, S.; Matsuo, Y.; Nakamura, E. Molecular and Supramolecular Control of the Work Function of an Inorganic Electrode with Self-Assembled Monolayer of Umbrella-Shaped Fullerene Derivatives. *J. Am. Chem. Soc.* **2011**, *133*, 16997−17004.
(71) Dhiman, S.; Ahmad, M.; Singla, N.; Kumar, G.; Singh, P.; Luxami, V.; Kaur, N.; Kumar, S. Chemodosimeters for optical detection of fluoride anion. *Coord. Chem. Rev.* **2020**, *405*, No. 213138.
(72) Qi, Y.; Cao, X.; Zou, Y.; Yang, C. Multi-resonance organoboron-based fluorescent probe for ultra-sensitive, selective and reversible detection of fluoride ions. *J. Mater. Chem. C* **2021**, *9*, 1567−1571.

(73) Saito, S.; Matsuo, K.; Yamaguchi, S. Polycyclic π-Electron System with Boron at Its Center. *J. Am. Chem. Soc.* **2012**, *134*, 9130−9133.
(74) Osumi, S.; Saito, S.; Dou, C.; Matsuo, K.; Kume, K.; Yoshikawa, H.; Awaga, K.; Yamaguchi, S. Boron-doped Nanographene: Lewis Acidity, Redox Properties, and Battery Electrode Performance. *Chem. Sci.* **2016**, *7*, 219−227.
(75) Matsuo, K.; Saito, S.; Yamaguchi, S. A Soluble Dynamic Complex Strategy for the Solution-Processed Fabrication of Organic Thin-Film Transistors of a Boron-Containing Polycyclic Aromatic Hydrocarbon. *Angew. Chem., Int. Ed.* **2016**, *55*, 11984−11988.
(76) Zhu, C.; Ji, X.; You, D.; Chen, T. L.; Mu, A. U.; Barker, K. P.; Klivansky, L. M.; Liu, Y.; Fang, L. Extraordinary Redox Activities in Ladder-Type Conjugated Molecules Enabled by B←N Coordination-Promoted Delocalization and Hyperconjugation. *J. Am. Chem. Soc.* **2018**, *140*, 18173−18182.
(77) Mula, S.; Leclerc, N.; Lévêque, P.; Retailleau, P.; Ulrich, G. Synthesis of Indolo[3,2-*b*]carbazole-Based Boron Complexes with Tunable Photophysical and Electrochemical Properties. *J. Org. Chem.* **2018**, *83*, 14406−14418.
(78) Li, G.; Chen, Y.; Qiao, Y.; Lu, Y.; Zhou, G. Charge Transfer Switching in Donor−Acceptor Systems Based on BN−Fused Naphthalimides. *J. Org. Chem.* **2018**, *83*, 5577−5587.
(79) Chen, Y.; Chen, W.; Qiao, Y.; Zhou, Gang B_2N_2-Embedded Polycyclic Aromatic Hydrocarbons with Furan and Thiophene Derivatives Functionalized in Crossed Directions. *Chem. − Eur. J.* **2019**, *25*, 9326−9338.
(80) Byrne, R.; Diamond, D. Chemo/bio-sensor networks. *Nat. Mater.* **2006**, *5*, 421−424.
(81) Wu, D.; Sedgwick, A. C.; Gunnlaugsson, T.; Akkaya, E. U.; Yoon, J.; James, T. D. Fluorescent chemosensors: the past, present and future. *Chem. Soc. Rev.* **2017**, *46*, 7105−7123.
(82) Griesbeck, S.; Zhang, Z.; Gutmann, M.; Lühmann, T.; Edkins, R. M.; Clermont, G.; Lazar, A. N.; Haehnel, M.; Edkins, K.; Eichhorn, A.; Desce, M. B.; Meinel, L.; Marder, T. B. Water-Soluble Triarylborane Chromophores for One- and Two-Photon Excited Fluorescence Imaging of Mitochondria in Cells. *Chem. − Eur. J.* **2016**, *22*, 14701−14706.
(83) Griesbeck, S.; Ferger, M.; Czernetzi, C.; Wang, C.; Bertermann, R.; Friedrich, A.; Haehnel, M.; Sieh, D.; Taki, M.; Yamaguchi, S.; Marder, T. B. Optimization of Aqueous Stability versus π-Conjugation in Tetracationic Bis(triarylborane) Chromophores: Applications in Live-Cell Imaging. *Chem. − Eur. J.* **2019**, *25*, 7679−7688.
(84) Ban, Ž.; Griesbeck, S.; Tomić, S.; Nitsch, J.; Marder, T. B.; Piantanida, I. A quadrupolar bis-triarylborane chromophore as a fluorimetric and chirooptic probe for simultaneous and selective sensing of DNA, RNA and proteins. *Chem. − Eur. J.* **2020**, *26*, 2195−2203.
(85) Still, W. C.; Kahn, M.; Mitra, A. Rapid chromatographic technique for preparative separations with moderate resolution. *J. Org. Chem.* **1978**, *43*, 2923−2925.

https://doi.org/10.1021/acs.chemmater.1c01441
Chem. Mater. 2021, 33, 5337−5344